

# Systematic Study of Podand Molecules for Synergistic Halogen and Hydrogen Bond-Driven Anion Recognition in the Solid State

Marco Saccone,<sup>\*[a]</sup> Massimo Cametti,<sup>[b]</sup> Pierangelo Metrangolo,<sup>\*[b]</sup> Tullio Pilati,<sup>[b]</sup>  
 Giuseppe Resnati,<sup>\*[b]</sup> and Giancarlo Terraneo<sup>[b]</sup>

**Abstract:** The increasing demand of species for the efficient capture and sensing of anions benefits from a systematic study of anion binding capabilities in the solid state. This work reports a detailed crystallographic study of ten structurally related podands and shows that these charged receptors

bind anions with a combination of charge-assisted halogen and hydrogen bonds. Computational tools helped in highlighting the role of the different involved interaction and afforded possible design principles for the design of improved podands.

## Introduction

The study of molecular recognition phenomena in the solid state and of the underlying intermolecular interactions driving the crystal packing is a well-established research field in supramolecular and materials chemistry.<sup>[1]</sup> In particular, it is well-known that the crystallization process by which molecules are mutually recognized and assembled into crystal is influenced by various parameters, such as molecular shape and volume, complementarity of molecular surfaces,<sup>[2]</sup> as well as by the effect of the specific non-covalent interactions.<sup>[3]</sup>

Anion binding is a classic theme in host-guest chemistry research. The presence of anionic species is ubiquitous in biological and abiotic systems and plays a central role in fields such as chemistry, biology, medicine and environmental science.<sup>[4,5]</sup> For example, phosphate and nitrate anions are involved in important environmental issues such as eutrophication.<sup>[6]</sup> Acetates are known to be key moieties in influencing the biochemical behavior of enzymes and antibodies,<sup>[7]</sup> and the delicate regulation of halides is crucial for the biosynthesis of hormones (iodide),<sup>[8]</sup> or for the prevention of cystic fibrosis (chloride).<sup>[9]</sup> Furthermore the sensing and capture of specific anions are also very important research fields impacting soil remediation and waste management. For example the detection and removal of the pertechnetate anion (containing the potent  $\beta$ -emitter <sup>99</sup>Tc) is becoming extremely important for nuclear waste management.<sup>[10]</sup>

Generally, the recognition of anions by synthetic receptors tries to mimic the natural systems where biomolecules use complex arrays of non-covalent interactions for the selective binding of these negatively charged units.<sup>[11]</sup> Over the years, a vast number of synthetic receptors with a large variety of molecular structures have been proposed and developed, extending the scale of the binding affinities towards anions. The recognition phenomenon between the anion and the receptor is usually driven by non-covalent interactions, such as charge-charge interactions, metal coordination, hydrogen bonds (HB), halogen bonds (XB), other  $\sigma$ -hole interactions and anion- $\pi$  interactions.<sup>[4,5]</sup> Thanks to the variety of the supramolecular tools available to researchers, different strategies for anion binding have been proposed, starting from the use of a single non-covalent interaction (*e.g.*, only HB) to the use of a combination of non-covalent interactions such as an anion- $\pi$  and a charge-charge interaction which may act alone or cooperatively. The latter approach has been largely applied in the past years showing that the use of multiple non-covalent interactions may indeed enhance the affinity and selectivity of the binding phenomena between the receptor and the anion. In this research area, the charged podand receptors based on 1,3,5-2,4,6-substituted benzenes have been widely used to bind ions thanks to the functionalization with different groups, as reported in pioneering papers by Raymond,<sup>[12]</sup> Anslyn,<sup>[13]</sup> and Steed.<sup>[14]</sup>

In line with this approach, we decided to develop a small library of podand receptors based on 1,3,5-2,4,6-functionalized benzenes (Figure 1) bearing halogen bonding and hydrogen bonding donor groups, with the aim of studying their ability to bind anions in the solid state. Here, we report on a comprehensive crystallographic and computational study of their anion binding capabilities investigating the binding role of halogen and hydrogen bonds.

Halogen bonding,<sup>[15]</sup> is a relatively recent addition to the toolbox of supramolecular chemistry,<sup>[16]</sup> which has been only exploited in the past ten years in the field of anion recognition.<sup>[17]</sup> Notably, several cases of podand receptors which have neutral or charged moieties bearing halogen bonding donor units have been reported<sup>[18–20]</sup>. For instance, Stilnović

[a] Dr. M. Saccone  
 Dipartimento di Ingegneria,  
 Università Degli Studi di Palermo,  
 Viale Delle Scienze, Edificio 6, Palermo, 90128 (Italy)  
 E-mail: marco.saccone@unipa.it

[b] Prof. M. Cametti, Prof. P. Metrangolo, T. Pilati, Prof. G. Resnati,  
 Prof. G. Terraneo  
 Dipartimento di Chimica Materiali e Ingegneria Chimica "Giulio Natta",  
 Politecnico di Milano,  
 Via Luigi Mancinelli 7, 20131, Milano (Italy)  
 E-mail: pierangelo.metrangolo@polimi.it  
 giuseppe.resnati@polimi.it

Supporting information for this article is available on the WWW under  
<https://doi.org/10.1002/asia.202201255>

This manuscript is part of a special collection on Halogen Bonding.

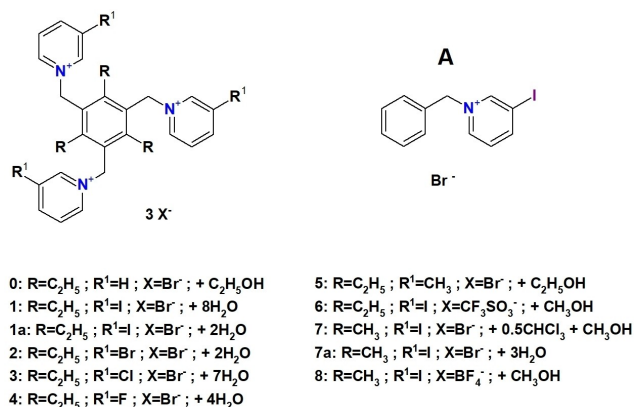


**Figure 1.** The podands studied in the present investigation. All the crystal structures show co-crystallized solvent molecules, whose nature and number are reported in the list.

*et al.*<sup>[21]</sup> evaluated a library of simple protonated or methylated halopyridinium iodides showing the effectiveness of these charged moieties to function as good XB donors towards the iodide ion in the solid state, while White *et al.* investigated iodo- and bromopyridinium based tripodal receptors highlighting their good binding affinities for the anion recognition even in solution.<sup>[22]</sup> In all the reported cases where a podand receptor was used, the structural orientation of the podand-arms played a key role. The spatial arrangement of the halopyridinium rings, namely up or down in relation to the plane described by the central aromatic ring, could be pre-organized, up to a certain extent, by varying the nature of the R groups (Figure 1) bonded to the benzene ring. This structural organization of the podand-arms could be and has been used to enhance the binding affinity toward anions. Indeed, it has been estimated that the alternating up and down (*ududud*) orientation of the podand-arms could lead to an energetic gain in the binding of about 15 kJ/mol.<sup>[23]</sup>

Motivated by these findings, we developed charged tripodal receptors combining hydrogen and halogen bonding donor groups in the 1,3,5-2,4,6-alkyl functionalized benzene core. In addition, we selected the ethyl unit as alkyl moiety linked to the central aromatic core since this should favor the preorganization of the system into a tripodal receptor featuring three chelating arms up. This pre-organization should promote the ability to bind the anionic substrates by a combination of charge assisted HBs and XBs.

In the following discussion, we present the investigation of a series of charged podand molecules featuring 3-substituted pyridinium arms capable of anion recognition in the solid state. The different interactions occurring in the systems studied were evaluated by means of Hirshfeld surface analysis,<sup>[24]</sup> and Interaction Region Indicator (IRI) analysis,<sup>[25]</sup> which helped us in highlighting the strengths and weaknesses of the podand design based on pyridinium arms in respect to other systems.

## Results and Discussion

**Materials Design.** The molecules studied in the present paper are depicted in Figure 1. We used the 1,3,5 tripyridinium-2,4,6-R (R = methyl or ethyl) benzene core. The pyridinium rings are in turn *meta* substituted with different groups, halogens (F, Cl, Br, I) and methyl. We also prepared the pyridinium salt **A**, deemed useful for comparison (ESI). The unsubstituted (H substituted) receptor **0** was already reported and will be only briefly discussed here.<sup>[14]</sup>

The anion receptors reported in this work were synthesized as bromide salts. Bromide (Br<sup>-</sup>) is a strong XB acceptor,<sup>[26]</sup> and an ideal candidate to explore the coordination of the receptors in the solid state. Nevertheless, other anions, such as triflate (OTf<sup>-</sup>) and tetrafluoroborate (BF<sub>4</sub><sup>-</sup>), which are more weakly coordinating than bromide,<sup>[27]</sup> were explored in combination with the strongest XB donors in our series: the *meta*-iodopyridinium receptor.

**Description of the X-ray structures, general considerations.** We studied a total of 10 crystal structures, which are reported here. We obtained two different solvated species of receptors **1** and **7**. Considering only the pyridinium moieties, the podand host assumes two basic conformations: the “three up” (3u), in which the three pyridinium arms are on the same side of the plane defined by the central benzene ring, and the “two up one down” (2u–1d). The hosts based on the 1,3,5-triethylbenzene scaffold **1–6** have additional conformations, based on the up or down conformations of the ethyl groups in respect to the pyridinium rings as reported by Hof.<sup>[23]</sup> In the following we will appoint with *u* or *d* the conformation of pyridinium moieties and *U* or *D* those of ethyl groups. In general, in the hosts having the 3u conformation, the three pyridinium arms form a cavity capped by one of the three anions, bonded by an array of CH<sub>arom</sub>...anion interactions, as in structures **1, 3, 4, 5** and **8**. No cavity is formed in the case of the 2u conformation, as in structures **1a, 2, 6,** and **8**. The other anions interact with the host molecules by anion...π, HB or XB and with the solvent molecules. Dispersive interactions among the podands and the anions, and among the podand molecules, are hardly understandable in terms of short contacts and are better visualized through the IRI analysis (see below). We describe these general features in detail for the structure **1** and briefly for the other structures.

**1:** The receptor adopts the stable *uDuDuD* conformation, with weakly distorted C<sub>3</sub> symmetry. As previously indicated, one of the bromide anions [Br(1), see Figure 2] caps the host’s cavity through six charge-assisted CH<sub>arom</sub> HB, where each ring acts as a bidentate donor. The observed C...Br<sup>-</sup> distances are in the range 3.462–3.861 Å. Similar CH...halide contacts were recently shown to be important in dictating the host-guest geometry in imidazolium-based hosts.<sup>[28]</sup> The coordination sphere of this Br<sup>-</sup> is completed by three water molecules (O...Br<sup>-</sup> distances being 3.326 1nd 3.330 Å) and by an additional HB with one aromatic ring of an adjacent receptor molecule. The Br(2) anion is halogen-bonded to iodine atoms on the pyridinium arms being the I(2) ...Br(2) length 3.179 Å and the C–I(2) ...Br(2) angle 178.43 °; here too the coordination sphere of the anion being

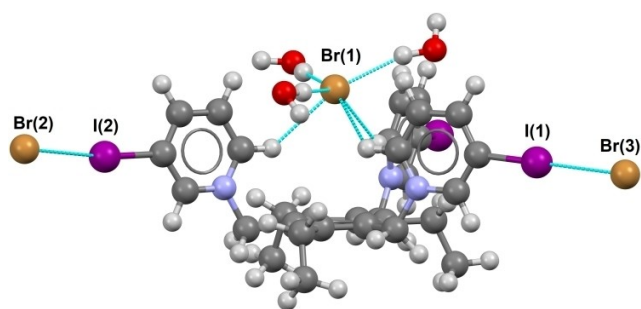


**Figure 2.** The asymmetric unit of the podand **1** shows the coordination of the bromide ion within the pre-organized cavity of the host and the main HB and XB of the structure, represented as cyan dotted lines. Color code: grey = C, white = H, red = O, blue = N, ocher = Br, purple = I.

completed by HB with different water molecules (the O...Br(2) distances span the range 3.428–3.463 Å). This bromide weakly interacts with a pyridinium ring, the distance between the anion and the centroid of the ring being 3.614 Å. The bromide Br(3) shows a weaker XB, the I(1)–Br(3) distance and the C–I(1)–Br(3) angle are 3.328 Å and 167.50°, respectively. This bromide anion shows only one HB with solvated H<sub>2</sub>O, the O–Br distance 3.278 being Å; its coordination sphere is completed by three podand molecules through two short contacts with CH moieties and two with CH<sub>2</sub> moieties.

**1a:** The receptor adopts a completely asymmetric *uDuDU* conformation.<sup>[23]</sup> The two up bromopyridinium arms point towards a single bromide giving two cooperative halogen bonds being I...Br distances 3.276–3.340 Å and C–I...Br angles 170.50–177.35° (Figure 3). The coordination sphere of this anion is completed by a charge assisted HB among three CH<sub>2</sub> involving three podand cations. The coordination spheres of the other two Br<sup>−</sup> anions are similar: in both cases two HB with solvated water are involved (O...Br distances are in the range 3.273–3.494 Å), further CH<sub>2</sub> and CH<sub>arom</sub> contacts with three podand molecules are also present.

**2:** This structure is isomorph to the structure **1a**, the difference being the substitution iodine/bromine atoms in pyridinium arms. The two cooperative halogen bonds show

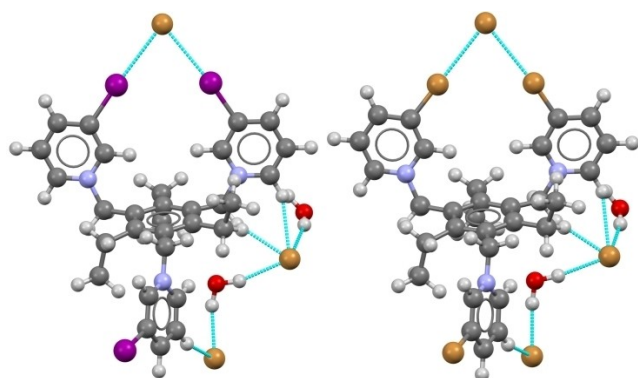


**Figure 3.** Comparison between the asymmetric units of the isostructural **1a** (left) and **2** (right). HB and XB are represented as cyan dotted lines. Color code: grey = C, white = H, red = O, blue = N, ocher = Br, purple = I.

about the same Br...Br distances and C–Br...Br angles as in **1a**, spanning the ranges 3.266–3.330 Å and 169.29–178.86°, respectively (Figure 3); also the four OH...Br contacts (in the range 3.262–3.498 Å) are very similar.

**3:** The receptor adopts an *uDuDU* conformation, with a strong deviation from the possible C<sub>3</sub> symmetry<sup>[23]</sup>. One Br<sup>−</sup> anion and one of the solvated water molecules are strongly disordered and were refined by splitting atoms over three positions with different population factor; the H atoms bonded to the disordered water molecule were not included. As it happens in **1**, one Br<sup>−</sup> anion caps the podand cavity with six C<sub>arom</sub>...Br distances in the range 3.501–3.709 Å. The coordination sphere of this Br<sup>−</sup> is completed by a HB with a solvated water molecule (O...Br distance 3.270 Å) and an XB with a chlorine atom, the Cl...Br distance and the C–Cl...Br angle being 3.335 Å and 171.46°, respectively. (Figure 4). The second ordered bromide anion shows two HB with solvated water molecules (O...Br distances 3.287 and 3.359 Å), an anion...π interaction, and other two short CH<sub>2</sub>...Br contacts with two different podand molecules. The large disorder of the third anions, lying in a large cavity of the structure, makes meaningless the discussion on its environment.

**4:** The podand molecule adopts the stable, nearly C<sub>3</sub>, *uDuDU* conformation as in **1**.<sup>[23]</sup> A bromide anion caps the cavity of the podand with six charge assisted hydrogen bonds, the H...Br distances being in the range 3.45–3.94 Å (Figure 4). The coordination sphere of this bromide is completed by two HB with solvated water molecules (O...Br distances 3.433 and 3.460 Å) and an anion...π interaction with a pyridinium moiety (the minimum Br...C<sub>arom</sub> distance is 3.163 Å). A second anion is linked by HB to two solvated water molecules (O...Br distances 3.247 and 3.437 Å); the coordination sphere is completed by anion...π interactions with two different pyridinium moieties (the shortest C...Br distances are 3.268–3.293 Å). This anion is also linked to a third podand through a charge assisted C–H<sub>arom</sub>...Br HB. Also the third bromide links two different podands by anion...π interactions (the shortest C...Br distances are 3.240–3.317 Å), and a third podand by a C–H<sub>arom</sub>...Br HB, but presents only one HB with solvated water molecules (O...Br distance 3.265 Å). No XB between fluorine atoms in the pyridinium ring and the Br<sup>−</sup> is present; probably the low polarizability of the fluorine atom makes the F...Br less favorable with respect to any H...Br contact. Notably, there are

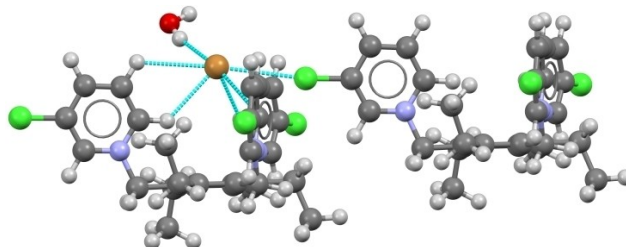


**Figure 4.** Partial coordination sphere of the bromide anion capping the cavity of podand **3** showing the C–Cl...Br XB from a neighboring podand molecule. Color code: grey = C, white = H, red = O, blue = N, green = Cl, ocher = Br.

two F...F short contacts with distances spanning the ranges 2.687–2.861 Å. The nature of these interactions is still under debate in the literature (Figure 5).<sup>[29]</sup>

5: The receptor adopts the uDuDuU conformation, showing nearly  $C_3$  symmetry. Here the three pyridinium arms adopt a T-shaped conformation (Figure 6). The structure contains completely disordered solvated ethanol; we were not able to establish the exact quantity of ethanol (and eventually of water) molecules really present. As usual for 3u conformation, a bromide anion caps the host's cavity interacting with it by six charge assisted hydrogen bonds with C...Br distances in the range 3.448–3.950 Å. The coordination sphere of such Br<sup>-</sup> is completed by contacts with a CH<sub>2</sub> and a CH<sub>3</sub> of two different podand molecules and with a disordered ethanol. A second bromide anion interacts with three podand molecules through two CH<sub>arom</sub>, two CH<sub>2</sub>, a CH<sub>3</sub>, and a  $\pi$  contact. The third Br<sup>-</sup> anion weakly interacts with four podand molecules through two CH<sub>arom</sub> and two CH; disordered ethanol completes its coordination sphere.

6: The receptor is completely asymmetric, with uDuDdU conformation<sup>[23]</sup>. One of the pyridinium up is disordered essentially for a small change of the C–CH<sub>2</sub>–N angle. Two of the three OTf<sup>-</sup> are strongly disordered. C–I bonds of the three arms point outwardly with respect to the benzene and all the three I

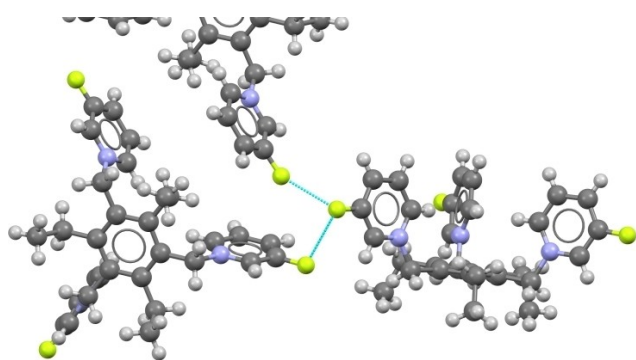


Figure 5. The F...F contacts in 4 (anions and solvent molecules are omitted for clarity). Color code: grey = C, white = H, red = O, blue = N, yellow = F.

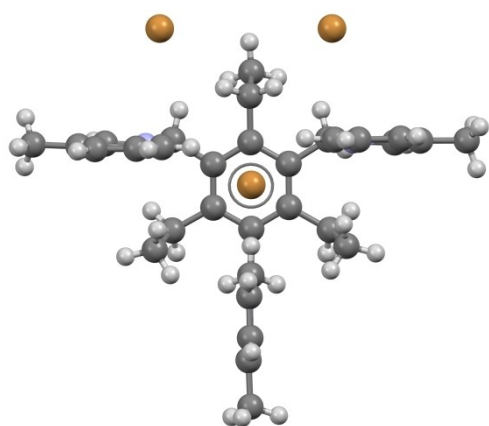


Figure 6. The asymmetric unit of the podand 5 showing nearly  $C_3$  symmetry. Disordered solvent is omitted for clarity. Color code: grey = C, white = H, blue = N, ocher = Br.

atoms are X-bonded to OTf<sup>-</sup> ions with O...I distances and O...I–C angles spanning the ranges 2.980–3.373 Å and 176.17–152.91 °, respectively. The podand is partially disordered: one of the pyridinium arms is split in two position with two slightly different C–N–C angles. One OTf<sup>-</sup> links by XB two podand molecules and is ordered, a second shows only one O...I contact and the third is not halogen-bonded to the podand; the last to OTf<sup>-</sup> are disordered over two positions each. Also, the molecule of methanol is disordered around the crystallographic center of symmetry (Figure 7).

7: At variance with host 1, 7 has methyl groups instead of ethyl groups on the benzene core. The podand cation shows the 2u–1d geometry. All the three iodine atoms are halogen bonded to Br<sup>-</sup> with C–I...Br distances and C–I...Br angles spanning the ranges 3.267–3.471 Å and 173.46–178.26 °, respectively. Notably, one bromide also interacts with the receptor by four charge-assisted CH<sub>arom</sub> hydrogen bonds (C...Br distances 3.400–3.506 Å). These H-bonds are formed with the two *u* arms of the podand. The coordination spheres of the three bromide anions are completed by several H-bonds established with MeOH solvent molecules and several CH...Br<sup>-</sup> contacts with neighboring podands (Figure 8).

7a: This structure is very similar to that of 7, the different crystallization conditions (H<sub>2</sub>O instead of CH<sub>3</sub>Cl/CH<sub>3</sub>OH) resulting in different solvent molecules in the crystal. Little differences between this structure and 7 are present in the pattern of HB between the solvent and the Br<sup>-</sup> anions (see Figure S3) One of the pyridinium arms shows the same type of disorder noted in 6. Due to the very low resolution of the data we were not able to refine the whole arm: only the iodine atom was split. Also, one of the bromide anions is disordered, being split on two site at 3.024 Å from a symmetry center where is located the third part of this anion. These three positions may be partially occupied by water, but the data quality does not allow for verifying this possibility.

8: This structure contains two independent podand molecules, namely A and B. A adopts the 2u–1d conformation, similar to that observed in receptor 7 while B adopts a 3u

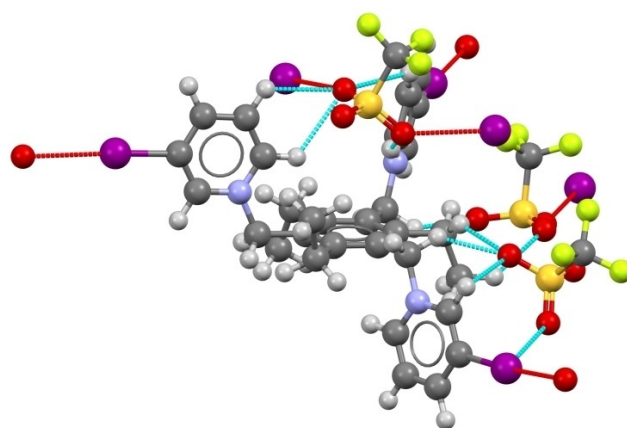
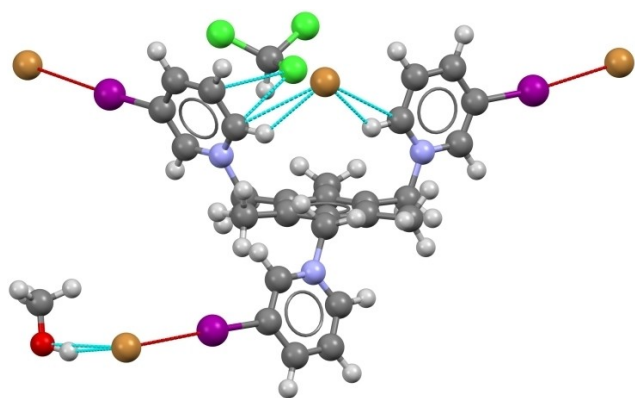
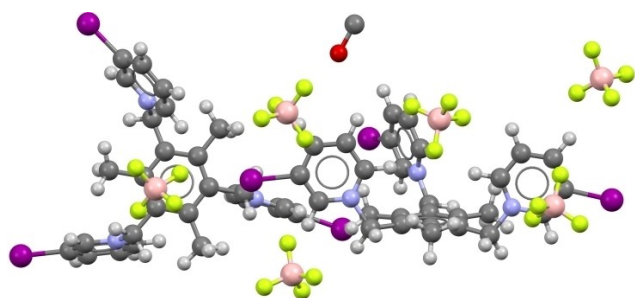


Figure 7. The asymmetric unit of podand 6 reveals a strong array of charge assisted HB and XB. HB and XB are represented as cyan and red dotted lines respectively. Color code: grey = C, white = H, red = O, blue = N, yellow = F, tan = S, purple = I, disorder is omitted for clarity.



**Figure 8.** The asymmetric unit of podand 7 reveals a strong array of charge assisted HB and XB. HB and XB are represented as cyan and red dotted lines respectively. Color code: grey = C, white = H, red = O, blue = N, yellow = F, green = Cl, ochre = Br, purple = I.

conformation: both the molecules are completely asymmetric. There are six independent  $\text{BF}_4^-$  anion units and all of them are linked by XB to the six independent iodine atoms; the F...I distances and F...I-C angles vary between 2.890-3.423 Å and 170.74-155.45°, respectively. Two  $\text{BF}_4^-$  anions are bridging couples of A and B podands, two link only one iodine atom; the other two show only CH...F contacts and only one interact also with a disordered solvate methanol molecule. One  $\text{BF}_4^-$  anion is located inside a cavity formed by podand B and interacts with it by charge assisted  $\text{CH}_{\text{arom}}$  hydrogen bonds with  $\text{CH}\cdots\text{F}\text{BF}_3^-$  distances in the range 3.07–3.36 Å (Figure 9).



**Figure 9.** The asymmetric unit of podand 8. Color code: grey = C, white = H, red = O, blue = N, yellow = F, pink = B, purple = I, disorder is omitted for clarity.

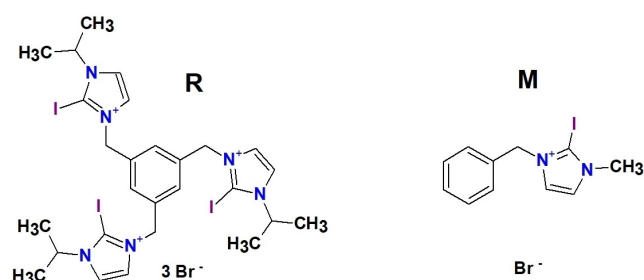


**Figure 10.** Chemical structure of R and M.

**Structure-property relationships.** The rationalization of the data from the obtained structures requires to mediate among the differences in the substitution pattern of the podands, their different conformations, and the different anion identity. We thus primarily focused on structures having the 3u conformation because of the importance of this conformation in the anion binding in solution.<sup>[14,30]</sup> We also compared our structures with the 2-iodoimidazolium based podand by Raatikainen *et al.*<sup>[31]</sup> (labeled R) and with the monodentate N-benzyl-iodopyridinium salt A, similar to that by Amendola *et al.*<sup>[32]</sup> with  $\text{Br}^-$  instead of  $\text{PF}_6^-$  as anion. We also discussed the monodentate N-benzyl-2-iodoimidazolium bromide salt M, similar to that of Cametti *et al.* (Figure 10).<sup>[28]</sup> The strategy to compare the present structures with similar systems reported in the literature aims at analyzing either the effect of the binding unit, pyridinium vs. imidazolium, and the effect of the platform – tripodal vs. free-standing binding unit.

As a start, we decided to perform Hirshfeld surface analysis.<sup>[24]</sup> As far as halogen... $\text{Br}^-$  contacts are concerned, we note a trend  $I_{(1)} > \text{Cl} > \text{F}$ , ( $I_{(1)}$  are the iodine atoms of 1) where iodine-containing receptor have the largest amount % of contacts which decreases along the series up to the fluorine-containing receptor (from 1.6 to 0.2%). This can be easily rationalized: first of all, the most polarizable and polarized halogen (iodine) has a higher tendency compared to the lighter halogens (chlorine and fluorine) to get involved in attractive XB interactions.<sup>[33]</sup> Secondly, the size of the halogen atom decreases from I to F so there is a higher probability for the bigger halogens to get involved in close contacts with the anion. Furthermore, XBs appear in structures 1 and 3 as distinct spikes in the fingerprint plots (Figure 11) while no spikes (non-bonding environment) are detected in the podand 4. In the comparison with A, the free standing iodopyridinium unit, however, we note that there is an increased amount of I... $\text{Br}^-$  contacts with respect to 1 (up to 1.9%). Finally, the shortest contacts and the more pronounced X... $\text{Br}^-$  spike belong to structure R, which appears by this first analysis to be the best XB donor (see below).

We also explored the distribution of both the length and the population of the  $\text{CH}\cdots\text{Br}^-$  contacts in the 3u podands 1, 3, 4, 5 and 8 and observed a nearly invariant role in the different receptors. This is a consequence of the design of reported podands: these systems are plus three charged species in which the  $\text{Br}^-$  is found to be inserted within the host cavity. Thus, in molecules having a similar conformation, a single atom mutation on the pyridinium ring does not allow for significant changes in the distribution and length of the  $\text{CH}\cdots\text{Br}^-$  contacts (found in the 12.4 to 10.8% range), which is instead probably just modulated by the nucleophilicity/electronegativity of the halogen (having an effect of the strength of HB). It is interesting to note, however, that the monodentate species A has indeed a decreased amount of  $\text{CH}\cdots\text{Br}^-$  contacts with respect to the podand 1 (8.3 vs 10.3%). As to R, the presence of  $\text{CH}\cdots\text{Br}^-$  interactions are in line with those in 1 (10.3 vs. 10.8%). Overall, these data suggest that the tripodal design limits the XB contribution to the binding in comparison to free-standing binding unit, as much as it increases that of CH HB sites.

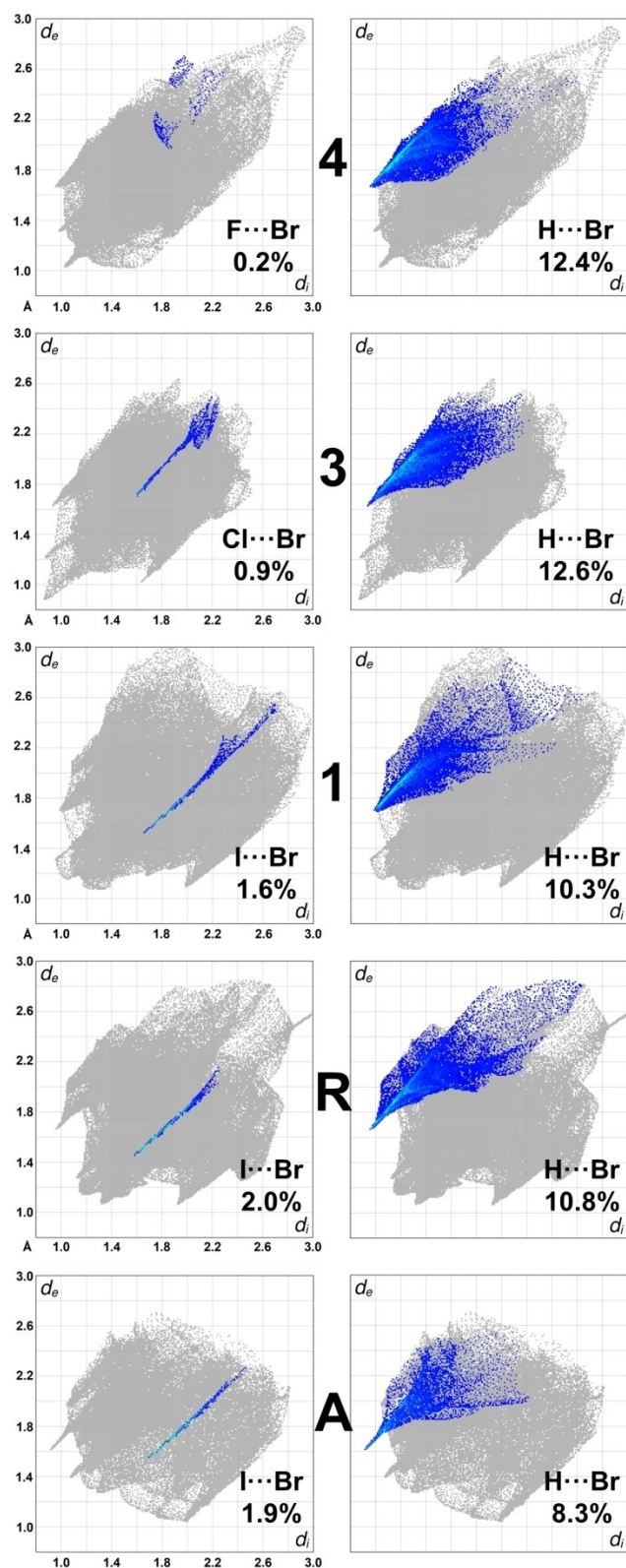


**Figure 11.** From up to down, fingerprint plots of the salts 4, 3, 1, R and A resolved into different interactions showing the percentages of contacts contributing to the total Hirshfeld surface area of the molecule. Distances are given in angstrom.

The fact that the anion recognition for these systems occurs inside the podand cavity<sup>[14]</sup> is both an advantage and a weakness of these systems. In fact, due to the limited size of the cavity which can be formed by using the 2,4,6-triethylbenzene core, small anions fit perfectly inside, however, due to the big size of heavier halogen atoms, their position in the pyridinium ring does not allow for a synergistic binding inside the cavity via XB. This also seems to be a general feature of tripodal system based on a 1,3,5 benzene trisubstituted platform (vide infra).

The geometrical description of the crystal structures used above, in which we identified short intermolecular contacts and described them as contributors to the overall crystal packing, is quite informative. However, this description gives only a partial picture about the factors that govern the crystal packing, and it is of limited help to identify the complete intermolecular landscape in solid-state structures. As stated before, the podand receptors are triply positively charged, so we expect significant electrostatic interactions. We clarified this point through the analysis of the electrostatic potential (ESP) surface  $V_s$  of the receptors which show some interesting features. This was done for structures 1, 3–4, for compounds R, A and M for the sake of comparison, and are reported in Figure 12.

As expected, the ESP is entirely positive in all the molecules, although we found important differences. First of all, the less positive regions of ESP in the podand receptors are located on

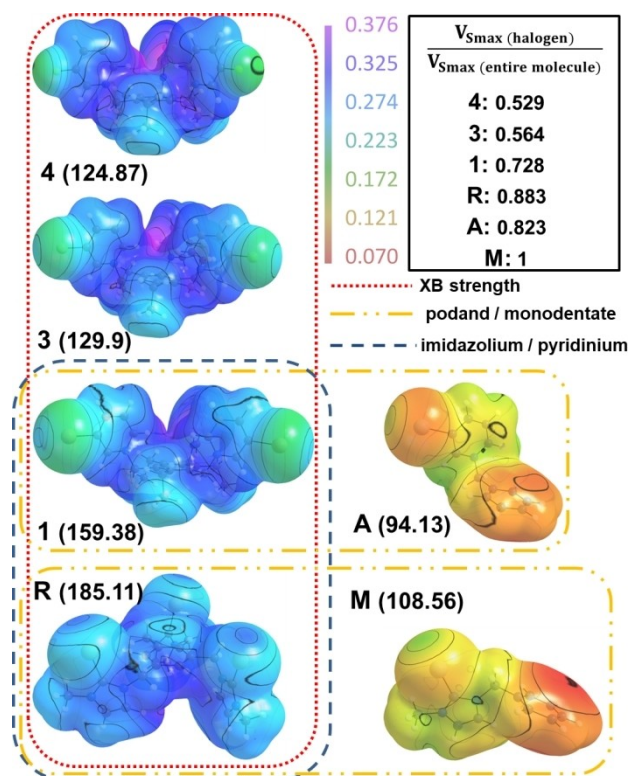


**Figure 12.** Comparisons of molecular electrostatic potentials (B3LYP aug-pcseg1) of the 1, 3–4, R, A and M salts plotted on the 0.001 au contour of the electron density.  $V_{s,max}$  (in kcal/mol) of halogen atoms are given in brackets. The electrostatic potential on the halogen atom gets higher, more positive, as its polarizability is increased.

the halogen atoms, in particular on the area which is approximately perpendicular to the C–X bond. This is due to the fact that halogens are among the most electronegative atoms and that they feature a considerable degree of polar flattening when attached to electron-deficient moieties.<sup>[34]</sup> Interestingly, in all cases within the tripodal compounds, the positive electrostatic potential along the extension of the C–X bond beyond the X atom (*viz.* “ $\sigma$ -hole”<sup>[35]</sup>) does not constitute the most positive area of the entire podand. Furthermore, in the fluorinated receptor **4**, there is virtually no difference in the local ESP of the F atoms, and the  $\sigma$ -hole develops in the order  $F < Cl < I_{(1)} < I_{(R)}$  (no  $\sigma$ -hole for F). Podand **R** appears to have the most positive values of  $V_{S,max}$  on its halogen atoms, and thus **R** might be a more effective XB donor compared to **1**. ESP studies were recently reported for simpler pyridinium salts,<sup>[21]</sup> and we thus included structures **A** and **M** in the EPS comparison. However, in these cases, absolute values are not meaningful as the total charge changes (triple vs. single). A way to circumvent this issue is to consider relative values: thus, we computed the ratio between the  $V_{S,max}$  at the halogen atom and the  $V_{S,max}$  of the entire molecule (Figure 12). This approach reveals that the monodentate **A** is an even better XB donor compared to the tripodal **1**. A similar behavior is revealed by the comparison of  $V_{S,max}$  of **R** and the  $V_{S,max}$  of **M**. It is interesting to note that the highest halogen  $V_{S,max}$  among the podand structures is shown by the iodine atoms in receptor **R** suggesting that iodoimidazolium cations are better XB donors compared to iodopyridinium cations, regardless of binding unit being free standing (as in **A** and **M**) or pre-organized onto a tripodal platform.

Finally, to better visualize the role of all of these interactions, we investigated selected structures by using Interaction-Region-Indicator (IRI) analysis and, in particular, the associated reduced density gradient (RDG) isosurfaces.<sup>[25]</sup>

IRI is defined as follows

$$IRI(r) = \frac{|\nabla\rho(r)|}{|\rho(r)|^\alpha}$$

where  $\rho$  is electron density,  $r$  is coordinate vector and  $\alpha$  is an adjustable parameter,  $\alpha = 1.1$  is adopted for standard definition of IRI. IRI is essentially the gradient norm of electron density weighted by scaled electron density. A visual explanation of what is visualized on IRI isosurfaces is given in Figure 13.

The main advantage of IRI or the related DORI,<sup>[36]</sup> compared to the NCI,<sup>[37]</sup> analysis is the possibility to simultaneously

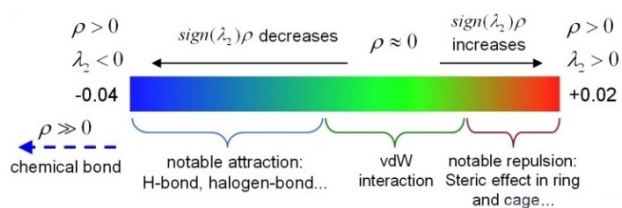


**Figure 13.** Details on how to interpret the role of different interactions visualized by means of the IRI analysis, together with their associated color code: strong HB and XB = blue, vdW = green, steric = tan to red.<sup>[25]</sup>

visualize both covalent bonds and non-covalent interactions. Specifically, we performed the IRI analysis to show the importance of non-covalent interactions such as charge assisted HB and XB, van der Waals (vdW) and to put in evidence the differences in the interaction pattern with anions other than  $Br^-$ .

Looking at the snapshots of the IRI isosurface of structure **1**, some things are evident. First of all, the bromide anion inside the cavity features several vdW interactions with the  $\pi$  cloud of the aromatic rings and weak  $CH\cdots Br^-$  HB as shown in Figure 14. Secondly, vdW forces –together with repulsive steric effects also exist which occur between the aromatic rings and ethyl groups, (Figure S1). Lastly, XB interactions (blue isosurfaces) are present between the I and Br atoms as shown in Figure 14b.

We performed IRI on structure **8** as well, and it reveals vdW interactions of the  $BF_4^-$  anion with the cavity and moderate HB with the *ortho*-pyridinium H atoms pointing inside the cavity as in Figure 15. XBs are also present in this structure, although we expect them to be weaker compared to those in **1** (Figure 14). This fact can be rationalized by the fact that  $BF_4^-$  is a lesser coordinating and less basic anion compared to  $Br^-$  and thus is expected to give weaker XB when the same XB donor is considered.<sup>[27]</sup>

The IRI analysis of structure **6** is reported in Figure 16. This structure features a 2u–1d conformation and thus no cavity is formed, nevertheless a  $OTf^-$  anion–Br is bound by vdW forces in the pseudo cavity formed by two iodopyridinium rings and the 2,4,6-triethylbenzene core.

Even in **6**, XB is present and the interaction of one of the iodine atoms with one oxygen of the  $OTf^-$  anion is highlighted in Figure 16. As it happens in **8**, these XB are expected to be weaker compared to the  $I\cdots Br^-$  interaction in **1** due to the fact that  $OTf^-$  is a weaker XB acceptor compared to  $Br^-$ .<sup>[27]</sup>

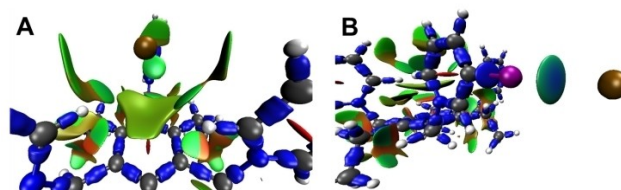


**Figure 14.** Isosurface maps of IRI = 1 of structure **1**. Maps follow the color code of Figure 13. A:  $Br^-$  inside the cavity, B:  $Br^-$  involved in XB interaction. Atoms color: H = white, C = grey, N = blue, Br = tan, I = purple.

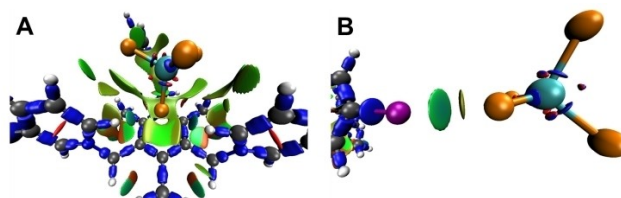


**Figure 15.** Isosurface maps of IRI = 1 of structure **8**. Maps follow the color code of Figure 12. A:  $BF_4^-$  inside the cavity, B:  $BF_4^-$  involved in XB interaction. Atoms color: H = white, B = cyan, C = grey, N = blue, F = orange, I = purple.

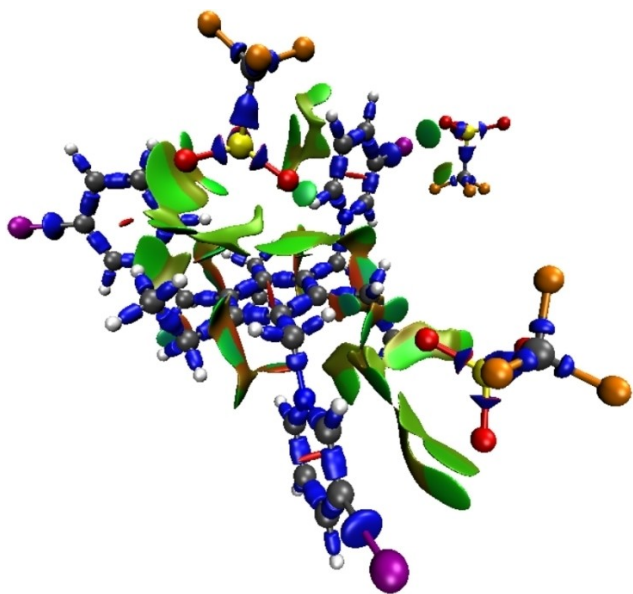


**Figure 16.** Isosurface maps of IRI = 1 of structure 6. Maps follow the color code of Figure 12. Atoms color: H = white, C = grey, N = blue, F = orange, S = yellow, I = purple.

Finally, we performed the IRI analysis on structure R (Figure S2) showing three strong XB between the iodine atoms and the Br<sup>-</sup> anions. These interactions are stronger compared to those present in structure 1.

Overall, the presented data show that in all the studied structures the binding occurs *via* a combination of vdW forces and charge assisted HB and XB. The XBs are less relevant ( $\sigma$ -hole less pronounced) in the pyridinium salts compared to the imidazolium salts, suggesting that imidazolium-based salts might be more effective in terms of XB contribution. Finally, both systems seem to be not optimal for boosting XB cooperative anion binding as the geometric constraint provided by the benzene platform makes the convergence of XB donor units towards a single anion impossible (Figure 17). This causes HB to outperform XB in binding an anion in the host cavity.

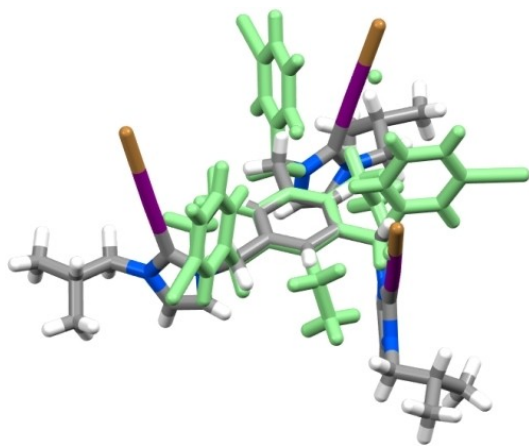


**Figure 17.** Capped sticks superimposition of receptors 1 and R. Color code: grey = C, white = H, red = O, blue = N, orange = Br, purple = I.

## Conclusion

Podand molecules represent a versatile platform for the design of anions receptors. In this work, we described a class of podands based on the 2,4,6-trisubstituted benzene core and carrying pyridinium arms. The features of these systems in terms of anion binding capability in the solid state is detailed. Analyses of short contacts indicates that anions are recognized by a combination of charge assisted HB and XB together with non-specific charge-charge interactions. Analysis of the ESP and IRI of selected podands confirmed these findings and, especially IRI, showed the presence of vdW interactions between the anion and the podand, especially when the former is bound by the podands cavity. Due to severe steric hindrance, XB does not participate in the binding of anions inside the cavity of a 3u receptor, however it is still an essential ingredient in the recognition of anions outside the cavity. The ESP and IRI analyses are found to be very informative in the understanding of the relative strength of HB and XB contributions and could be used for the design of future XB based receptors.

## Experimental Section

**Synthesis.** Anion receptors **A**, **1,2,3,4,5** and **7** were synthesized adapting the methodology reported by Steed.<sup>[38]</sup> The chosen 3-substituted pyridine and 1,3,5-tri(bromomethyl)-2,4,6-triethylbenzene, benzyl bromide, or 1,3,5-tri(bromomethyl)-2,4,6-trimethylbenzene, were placed in a 5 ml grinding jar on a ball mill and ground at 30 Hz for 90 min. We found that this protocol works also for pyridine derivatives with severely electron-withdrawing substituents such as fluorine. The resulting solid (200 mg scale) was washed twice with 1 ml of chloroform and collected by filtration to afford the pure products. In all cases the yields are equal or greater than 90%. Compounds **6** and **8** were prepared from **1** and **7** by solution phase anion metathesis with silver triflate and silver tetrafluoroborate respectively. The metathesis was performed in water and the precipitate of silver bromide was carefully separated from the solution by centrifugation, washed with methanol, to extract the residual compounds and discarded. After evaporation of the water/methanol liquors, the compounds **6** and **8** were obtained in 83% and 76% yield respectively.

**Computational Details.** Calculations were performed on a laptop equipped with an Intel® Core™ i7-8750H Processor and 32 GB RAM. The Hirshfeld surface analysis was performed with the CrystalExplorer17 suite of programs,<sup>[39]</sup> while the Interaction Region Indicator (IRI) analysis was performed with the Multiwfn 3.8 software,<sup>[40]</sup> coupled with VMD 1.9 as visualization software.<sup>[41]</sup> Electron densities for the IRI analysis and electrostatic potentials were obtained at the DFT level with the GAUSSIAN 09 W suite of programs,<sup>[42]</sup> using the B3LYP functional,<sup>[43]</sup> and the aug-pcseg1 (superior to the aug-cc-pVDZ) basis set of Jansen optimized for DFT calculations,<sup>[44]</sup> except for iodine atoms, for which the DGDZVP basis set was used.<sup>[45]</sup> Geometries were taken from crystallographic coordinates. Before the single-point energy calculations at the experimental geometry started, C–H bond distances were restrained to the values obtained from neutron diffraction studies of small molecules.<sup>[46]</sup> The electrostatic potentials were visualized using the software MoleCoolQt.<sup>[47]</sup>

**X-ray Crystallography.** The single crystal X-ray structure were determined on a Bruker Kappa Apex II diffractometer at 103 K using a fine-focus MoK $\alpha$  tube,  $\lambda = 0.71073$  Å. Data collection and

reduction were performed by SaintPlus 6.01,<sup>[48]</sup> and absorption correction, based on multi-scan procedure, by SADABS.<sup>[49]</sup> The structure was solved by SIR92,<sup>[50]</sup> and refined on all independent reflections by full-matrix least-squares based on  $F_o^2$  by using SHELX-97.<sup>[51]</sup> All the non-hydrogen atoms were refined anisotropically. Hydrogen atoms were assigned to idealized positions and were allowed to ride. The structures were registered in the Cambridge Structural Database, see Table S1 for details.

## Acknowledgements

Marco Saccone acknowledges PON R&I 2014–2020 – AIM (Attraction and International Mobility), project AIM 1813040 for financial support.

## Conflict of Interest

The authors declare no conflict of interest.

## Data Availability Statement

The data that support the findings of this study are available in the supplementary material of this article.

**Keywords:** Anion Receptor · Hydrogen Bond · Halogen Bond · Self-Assembly · Supramolecular Chemistry

- [1] G. R. Desiraju, J. J. Vittal, A. Ramanan, *Crystal Engineering*, World Scientific, Singapore, 2011.
- [2] A. I. Kitaigorodskii, *Molecular Crystals and Molecules*; Academic Press, 1973.
- [3] J. J. Novoa, *Intermolecular Interactions in Crystals: Fundamentals of Crystal Engineering*, Royal Society of Chemistry, Cambridge, 2018.
- [4] N. H. Evans, P. D. Beer, *Angew. Chem. Int. Ed.* **2014**, *53*, 11716–11754; *Angew. Chem.* **2014**, *126*, 11908–11948.
- [5] N. Busschaert, C. Caltagirone, W. Van Rossom, P. A. Gale, *Chem. Rev.* **2015**, *115*, 8038–8155.
- [6] M. Le Moal, C. Gascuel-Oudou, A. Ménesguen, Y. Souchon, C. Étrillard, A. Levain, F. Moatar, A. Pannard, P. Souchu, A. Lefebvre, G. Pinay, *Sci. Total Environ.* **2019**, *651*, 1–11.
- [7] M. Cox, D. Nelson, *Lehninger Principles of Biochemistry* Macmillan, 2021.
- [8] M. B. Zimmermann, P. L. Jooste, C. Pandav, *Lancet* **2008**, *372*, 1251–1262.
- [9] M. P. Anderson, R. J. Gregory, S. D. Thompson, W. Souza, S. Paul, R. C. Mulligan, A. E. Smith, M. J. Welsh, *Science* **1991**, *253*, 202–205.
- [10] D. Banerjee, D. Kim, M. J. Schweiger, A. A. Kruger, P. K. Thallapally, *Chem. Soc. Rev.* **2016**, *45*, 2724–2739.
- [11] O. Hayashida, A. Shivanyuk, J. Rebek, *Angew. Chem. Int. Ed.* **2002**, *41*, 3423–3426; *Angew. Chem.* **2002**, *114*, 3573–3576.
- [12] T. D. P. Stack, Z. Hou, K. N. Raymond, *J. Am. Chem. Soc.* **1993**, *115*, 6466–6467.
- [13] G. Hennrich, E. V. Anslyn, *Chem. Eur. J.* **2002**, *8*, 2218–2224.
- [14] K. J. Wallace, W. J. Belcher, D. R. Turner, K. F. Syed, J. W. Steed, *J. Am. Chem. Soc.* **2003**, *125*, 9699–9715.
- [15] G. R. Desiraju, P. S. Ho, L. Kloo, A. C. Legon, R. Marquardt, P. Metrangolo, P. Politzer, G. Resnati, K. Rissanen, *Pure Appl. Chem.* **2013**, *85*, 1711–1713.
- [16] M. Saccone, L. Catalano, *J. Phys. Chem. B* **2019**, *123*, 9281–9290.
- [17] A. Brown, P. D. Beer, *Chem. Commun.* **2016**, *52*, 8645–8658.
- [18] A. Mele, P. Metrangolo, H. Neukirch, T. Pilati, G. Resnati, *J. Am. Chem. Soc.* **2005**, *127*, 14972–14973.
- [19] M. G. Sarwar, B. Dragisic, S. Sagoo, M. S. Taylor, *Angew. Chem. Int. Ed.* **2010**, *49*, 1674–1677; *Angew. Chem.* **2010**, *122*, 1718–1721.
- [20] L. C. Gilday, N. G. White, P. D. Beer, *Dalton Trans.* **2013**, *42*, 15766–15773.
- [21] L. Fotović, N. Bedeković, V. Stilinović, *Cryst. Growth Des.* **2021**, *21*, 6889–6901.
- [22] E. M. Foyle, N. G. White, *CrystEngComm* **2020**, *22*, 2526–2536.
- [23] X. Wang, F. Hof, *Beilstein J. Org. Chem.* **2012**, *8*, 1.
- [24] M. A. Spackman, D. Jayatilaka, *CrystEngComm* **2009**, 19–32.
- [25] T. Lu, Q. Chen, *Chem. Methods* **2021**, 231–239.
- [26] P. Metrangolo, T. Pilati, G. Terraneo, S. Biella, G. Resnati, *CrystEngComm* **2009**, *11*, 1187–1196.
- [27] I. M. Riddlestone, A. Kraft, J. Schaefer, I. Krossing, *Angew. Chem. Int. Ed.* **2018**, *57*, 13982–14024; *Angew. Chem.* **2018**, *130*, 14178–14221.
- [28] M. Cametti, K. Raatikainen, P. Metrangolo, T. Pilati, G. Terraneo, G. Resnati, *Org. Biomol. Chem.* **2012**, *10*, 1329–1333.
- [29] A. Varadwaj, H. M. Marques, P. R. Varadwaj, *Molecules* **2019**, *24*, 379–407.
- [30] O. B. Berryman, A. C. Sather, B. P. Hay, J. S. Meisner, D. W. Johnson, *J. Am. Chem. Soc.* **2008**, *130*, 10895–10897.
- [31] K. Raatikainen, G. Cavallo, P. Metrangolo, G. Resnati, K. Rissanen, G. Terraneo, *Cryst. Growth Des.* **2013**, *13*, 871–877.
- [32] V. Amendola, G. Bergamaschi, M. Boiocchi, N. Fusco, M. V. La Rocca, L. Linati, E. Lo Presti, M. Mella, P. Metrangolo, A. Miljkovic, *RSC Adv.* **2016**, *6*, 67540–67549.
- [33] P. Politzer, J. S. Murray, T. Clark, *Phys. Chem. Chem. Phys.* **2010**, *12*, 7748–7757.
- [34] A. J. Stone, *J. Am. Chem. Soc.* **2013**, *135*, 7005–7009.
- [35] T. Clark, *WIREs Comput. Mol. Sci.* **2013**, *3*, 13–20.
- [36] P. De Silva, C. Corminboeuf, *J. Chem. Theory Comput.* **2014**, *10*, 3745–3756.
- [37] E. R. Johnson, S. Keinan, P. Mori-Sánchez, J. Contreras-García, A. J. Cohen, W. Yang, *J. Am. Chem. Soc.* **2010**, *132*, 6498–6506.
- [38] A. Swinburne, J. W. Steed, *CrystEngComm* **2009**, *11*, 433–438.
- [39] M. J. Turner, J. J. McKinnon, S. K. Wolff, D. J. Grimwood, P. R. Spackman, D. Jayatilaka, M. A. Spackman, University of Western Australia, 2017.
- [40] T. Lu, F. W. Chen, *J. Comput. Chem.* **2012**, *33*, 580–592.
- [41] W. Humphrey, A. Dalke, K. Schulten, *J. Mol. Graphics* **1996**, *14*, 33–38.
- [42] M. J. Frisch, G. W. Trucks, H. B. Schlegel, G. E. Scuseria, M. A. Robb, J. R. Cheeseman, G. Scalmani, V. Barone, B. Mennucci, G. A. Paterson, H. Nakatsuji, M. Caricato, X. Li, H. P. Hratchian, A. F. Izmaylov, J. Bloino, G. Zheng, J. L. Sonnenberg, M. Hada, M. Ehara, K. Toyota, T. R. Fukuda, J. Hasegawa, M. Ishida, T. Nakajima, Y. Honda, O. Kitao, H. Nakai, T. Vreven, K. Throssell, J. A. J. Montgomery, J. E. Peralta, F. Ogliaro, M. Bearpark, J. J. Heyd, E. Brothers, K. N. Kudin, V. N. Staroverov, R. Kobayashi, J. Normand, K. Raghavachari, A. Rendell, J. C. Burant, S. S. Iyengar, J. Tomasi, M. Cossi, N. Rega, J. M. Millam, M. Klene, J. E. Knox, J. B. Cross, V. Bakken, C. Adamo, J. Jaramillo, R. E. Stratmann, R. Gomperts, O. Yazyev, A. J. Austin, R. Cammi, C. Pomelli, J. W. Ochterski, R. L. Martin, K. Morokuma, V. G. Zakrzewski, G. A. Voth, P. Salvador, J. J. Dannenberg, S. Dapprich, A. D. Daniels, O. Farkas, J. B. Foresman, J. V. Ortiz, J. Cioslowski, D. J. Fox, *Gaussian09, Revision C.01*, Gaussian Inc., Wallingford, 2009.
- [43] A. D. Becke, *J. Chem. Phys.* **1993**, *98*, 5648.
- [44] F. Jensen, *J. Chem. Theory Comput.* **2014**, *10*, 1074–1085.
- [45] C. Sosa, J. Andzelm, B. C. Elkin, E. Wimmer, K. D. Dobbs, D. A. Dixon, *J. Phys. Chem.* **1992**, *96*, 6630–6636.
- [46] F. H. Allen, I. Bruno, *Acta Crystallogr. Sect. B* **2010**, *66*, 380–386.
- [47] C. B. Hubschle, B. Dittrich, *J. Appl. Crystallogr.* **2011**, *44*, 238–240.
- [48] Saint Plus, v.6.01; Bruker Analytical X-Ray Systems: Madison, WI, 1999.
- [49] G. M. Sheldrick, SADABS: Empirical Absorption Correction Program; University of Gottingen, Germany, 2001.
- [50] A. Altomare, G. Cascarano, C. Giacovazzo, A. Guagliardi, M. C. Burla, G. Polidori, M. Camalli, *J. Appl. Crystallogr.* **1994**, *27*, 435.
- [51] G. M. Sheldrick, SHELXS-97 and SHELXL-97, Program for Crystal Structure Solution and Refinement. University of Gottingen, Gottingen, 1997.

Manuscript received: December 16, 2022

Revised manuscript received: January 25, 2023

Accepted manuscript online: January 30, 2023

Version of record online: February 7, 2023